THE ASTROPHYSICAL JOURNAL, 548:47–59, 2001 February 10

NONLINEAR GRAVITATIONAL GROWTH OF LARGE-SCALE STRUCTURES INSIDE AND OUTSIDE STANDARD COSMOLOGY

E. GAZTAÑAGA[1,2] AND J. A. LOBO[3]

Received 2000 July 19; accepted 2000 October 4

ABSTRACT

We reconsider the problem of gravitational structure formation inside and outside general relativity (GR), in both the weakly and strongly nonlinear regime. We show how these regimes can be explored observationally through clustering of high-order cumulants and through the epoch of formation, abundance, and clustering of collapse structures, using Press-Schechter formalism and its extensions. We address the question of how different these predictions are when using a nonstandard theory of gravity. We study examples of cosmologies that do not necessarily obey Einstein's field equations: scalar-tensor theories (STT), such as Brans-Dicke (BD), parametrized with ω, a nonstandard parameterization of the Hubble law, $H^2 = a^{-3(1+\epsilon)}$, or a nonstandard cosmic equation of state $p = \gamma\rho$, where γ can be chosen irrespective of the cosmological parameters (Ω_M and Ω_Λ). We present some preliminary bounds on γ, ω, and ϵ from observations of the skewness and kurtosis in the Automated Plate Measuring (APM) Galaxy Survey. This test is independent of the overall normalization of rms fluctuations. We also show how abundances and formation times change under these assumptions. Upcoming data on nonlinear growth will place strong constraints on such variations from the standard paradigm.

Subject headings: galaxies: formation — gravitation — instabilities — large-scale structure of universe

1. INTRODUCTION

In cosmology, the standard picture of gravitational growth, and also many aspects of fundamental physics, are extrapolated many orders of magnitude from the scales and times at which our current theory of gravity (general relativity, GR) has been experimentally tested, into the distant universe. In particular, current limits on the (parametrized) post-Newtonian formalism are mostly restricted to our very local universe (see Will 1993). It is important to evaluate how much our predictions and cosmological picture depend on the underlying hypothesis (see Peebles 2000 for insightful comments on the state of this subject). The other side of this argument is that cosmology can be used to test fundamental physics, such as our theory of gravity.

One aspect of GR that could be questioned or tested without modifying the basic structure or symmetry of the theory are Einstein's field equations, relating the energy content ($T_{\mu\nu}$) to the curvature ($R_{\mu\nu}$). One such modification, which will be considered here, is scalar-tensor theories (STT), such as the Brans-Dicke (BD) theory. A more generic, but also more vague, way of testing the importance of Einstein's field equations is to independently model the geometry and the matter content, thus allowing for the possibility of other relations between them. Some simple aspects of this idea will be illustrated here by studying structure formation in a flat, matter-dominated universe, but with a more general growth law for the Hubble rate (see § 3.2). Similarly, we will also consider results for a generic equation of state: $p = \gamma\rho$, where γ can be chosen independently of the cosmological parameters (Ω_M, Ω_k, and Ω_Λ).

Our aim in this paper is to explore certain variations of the standard model to see how they affect structure formation. The idea is to find a way to parameterize variations from GR that might produce differences large enough to be observable. The variations considered could have other observable consequences (e.g., in the local universe or in the radiation-dominated regime) which might rule them out as a viable new theory. But even if this were the case, we still would have learned something about how structure formation depends on the underlying theory of gravity or the assumptions about the equation of state. This aspect of the theory has hardly been explored, and it therefore represents an important step forward in analyzing alternatives to the current paradigm, e.g., nonbaryonic matter (see Peebles 2000), and could also help to set limits on variations of GR or the equation of state at high redshifts.

Here we consider two main regimes for structure formation in nonstandard gravity/cosmology: weakly nonlinear and strongly nonlinear large-scale clustering. We study the shear-free or spherical collapse (SC) model, which corresponds to the spherically symmetric (or local) dynamics (see below). This approximation works very well in at least two different contexts that will be explored here.

The first scenario is the growth of the smoothed one-point cumulants of the probability distribution for large-scale density fluctuations: the SC model turns out to reproduce exactly the leading-order perturbation-theory predictions (Bernardeau 1992), and turns out to be an excellent approximation for the exact dynamics as compared to N-body simulations with both Gaussian (Fosalba & Gaztañaga 1998a, 1998b) and non-Gaussian initial conditions (Gaztañaga & Fosalba 1998). The measured one-point cumulants in galaxy catalogs have been compared with these predictions (e.g., Bouchet et al. 1993; Gaztañaga 1992, 1994, 1995; Gaztañaga & Frieman 1994; Baugh, Gaztañaga, & Efstathiou 1995; Baugh & Gaztañaga 1996; Colombi et al. 1997; Hui & Gaztañaga 1999).

The second scenario is the study of the epoch of formation and abundance of structures (such as galaxies and clusters), using the Press & Schechter (1974) formalism and its extensions (e.g., Bond et al. 1991; Lacey & Cole 1993;

[1] INAOE, Astrofisica, Tonantzintla, Apdo Postal 216 y 51, 7200, Puebla, Mexico; gazta@inaoep.mx.
[2] Institut d'Estudis Espacials de Catalunya, IEEC/CSIC, Gran Capitán 2-4, 08034 Barcelona, Spain; gaztanaga@ieec.fcr.es.
[3] Departament de Fisica Fonamental, Universitat de Barcelona, Diagonal 647, 08028 Barcelona, Spain; lobo@ffn.ub.es.

Sheth & Lemson 1999; Scoccimarro et al. 2000). Given some Gaussian initial conditions, this formalism can predict the number of structures (halos) of a given mass that will form at each stage of the evolution. One can use the SC model to predict the value of the critical linear overdensity, δ_c, that will collapse into virialized halos. It turns out that the analytical predictions for the halo mass function and formation rates are remarkably accurate as compared to N-body simulations (Lacey & Cole 1994). One can also use this type of modeling to predict clustering properties of halos (e.g., Mo & White 1996; Mo, Jing, & White 1997), cluster abundances (White, Efstathiou, & Frenk 1993; Bahcall & Fan 1998), or weak lensing through mass functions (Jain & Van Waerbeke 2000). The observed cluster abundances have been used as a strong discriminant for cosmological models and also as a way to measure the amplitude of mass fluctuations, σ_8 (see White et al. 1993; Bahcall & Fan 1998).

In summary, we propose to address a very specific question here: how different are the above nonlinear predictions when using a nonstandard cosmology and nonstandard theory of gravity? To answer this question, we consider two nonstandard variations: scalar-tensor models and some examples of a cosmology that do not obey Einstein's field equations. The paper is organized as follows. In § 2 we give a summary of how nonlinear structure formation relates to the underlying theory of gravity (see Weinberg 1972; Peebles 1993; Ellis 1999, and references therein for a review of the relation between gravitational theory and cosmology). This section covers old ground with some detail, as an introduction to later sections and for the reader who is not familiar with this subject or notation. We also present the more general case of an ideal (relativistic) fluid. As far as we know, some of the nonlinear results presented here are new. In § 3 we show how these predictions change in the two examples of nonstandard gravity. Observational consequences are explored in § 4. In § 5 we present a discussion and our conclusions.

2. GRAVITATIONAL GROWTH INSIDE GR

The self-gravity of an overdense region works against the expansion of the universe, so that this region will expand at a slower rate that the background. This increases the density contrast, so that eventually the region collapses. The details of this collapse depend on the initial density profile. Here we focus on the spherically symmetric case. We revise nonlinear structure growth in the context of the fluid limit and the shear-free approximation. These turn out to be very good approximations for the applications that will be considered later (leading-order and strongly nonlinear statistics).

We start with Raychaudhuri's equation, which is valid for an arbitrary Ricci tensor $R_{\mu\nu}$. We use Einstein's field equations and the continuity equation to turn Raychaudhuri's equation into a second-order differential equation for the density contrast. We first present the matter-dominated (nonrelativistic) case, with solutions for the linear and nonlinear regimes. Later, in § 2.5, we assess the more generic case of an ideal (relativistic) fluid and its corresponding solution.

2.1. *Einstein's and Raychaudhuri's Equations*

We start by recalling that the metric tensor $g_{\mu\nu}$ defines the line element of spacetime:

$$ds^2 = g_{\mu\nu}\, dx^\mu\, dx^\nu\,, \tag{1}$$

which in the homogeneous and isotropic model of the cosmological principle can be written as (see, e.g., Weinberg 1972)

$$ds^2 = dt^2 - a^2(t)\left[\frac{dr^2}{1+kr^2} + r^2(d\theta^2 + \sin^2\theta\, d\phi^2)\right]. \tag{2}$$

As usual, we work in comoving coordinates $\boldsymbol{x}$ related to physical coordinates by $\boldsymbol{r}_p = a(t)\boldsymbol{x}$, where $a(t) = (1+z)^{-1}$ is the cosmic scale factor, and z the corresponding redshift ($a_0 \equiv 1$). Thus, all geometrical aspects of this universal line element are determined up to the function $a(t)$ and the arbitrary constant k, which defines the usual open, Einstein–de Sitter, and closed universes. The function $a(t)$ can be found for each energy content by solving the corresponding equations of motion, e.g., the gravitational field equations.

In this section we consider Einstein's equations,

$$R_{\mu\nu} + \Lambda g_{\mu\nu} = -8\pi G(T_{\mu\nu} - \tfrac{1}{2} g_{\mu\nu}\, T)\,, \tag{3}$$

where $T \equiv g^{\mu\nu}T_{\mu\nu}$ is the trace of the energy-momentum tensor; we have included a cosmological constant term to keep the equations general at this stage. For an ideal fluid, we have

$$T_{\mu\nu} = p g_{\mu\nu} + (p+\rho) u_\mu u_\nu\,. \tag{4}$$

We can now use the field equations and the above energy-momentum to find the scale factor $a(t)$ in the metric

$$\frac{3}{a}\,\ddot{a} = -4\pi G\rho\left(1 + \frac{3p}{\rho}\right) + \Lambda \tag{5}$$

$$H^2 \equiv \frac{\dot{a}^2}{a^2} = \frac{8\pi G\rho}{3} + \frac{k}{a^2} + \frac{\Lambda}{3}\,, \quad \text{overdot} \equiv \frac{d}{dt}\,. \tag{6}$$

In the fluid approximation, deviations from the mean background $\overline{\rho}$ are characterized by fluctuations in the density and velocity fields. The continuity equation for a nonrelativistic fluid is (Peebles 1993)

$$\frac{\partial}{\partial\tau}\,\delta(\boldsymbol{x},\tau) + \boldsymbol{\nabla}\cdot\{[1+\delta(\boldsymbol{x},\tau)]\boldsymbol{v}(\boldsymbol{x},\tau)\} = 0\,, \tag{7}$$

where $\delta(\boldsymbol{x},\tau) \equiv \rho(\boldsymbol{x},\tau)/\overline{\rho} - 1$ is the local density contrast, $\boldsymbol{v}(\boldsymbol{x},\tau)$ is the peculiar velocity (see eq. [11] below), and τ is the conformal time, defined by

$$d\tau = \frac{dt}{a(t)} \Leftrightarrow \frac{d}{dt} = \frac{1}{a}\frac{d}{d\tau}\,. \tag{8}$$

The continuity equation (7) can also be written

$$\frac{d\delta}{d\tau} + (1+\delta)\theta = 0\,, \quad \theta \equiv \boldsymbol{\nabla}\cdot\boldsymbol{v}\,. \tag{9}$$

In order to find an equation of motion for the density contrast alone, we resort to the Raychaudhuri equation (see, e.g., Wald 1984),

$$\frac{d\Theta}{ds} + \frac{1}{3}\,\Theta^2 = -\sigma_{ij}\sigma^{ij} + \omega_{ij}\omega^{ij} + R_{\mu\nu}u^\mu u^\nu\,, \tag{10}$$

where $\Theta \equiv \nabla_\mu u^\mu$, σ_{ij} is the shear tensor, ω_{ij} is the vorticity tensor, $R_{\mu\nu}$ is the Ricci tensor, and s is the proper time parameter; u^μ is the fluid's 4-velocity, $u^0 = 1$, and

$$\boldsymbol{u} = \dot{a}(t)\boldsymbol{x} + \boldsymbol{v}(\boldsymbol{x},t)\,. \tag{11}$$

It is important to stress that Raychaudhuri's equation, equation (10), is *purely geometric*: it describes the evolution in proper time of the dilatation coefficient Θ of a bundle of nearby geodesics. There is no physics in this equation until a relationship between $R_{\mu\nu}$ and the matter contents of the universe is specified by means of a set of field equations. This makes it very useful for our purposes in this paper, since we later make reference to a different set of field equations.

If Einstein's field equations, equations (3) and (4), are assumed, then it is readily verified that

$$R_{\mu\nu}u^\mu u^\nu = -4\pi G\rho\left(1+\frac{3p}{\rho}\right)+\Lambda\,. \tag{12}$$

2.2. *Shear-Free and Matter Domination*

In a matter-dominated regime ($p=0$), $\rho\sim a^{-3}$. Equation (6) for the Hubble rate H can be rewritten using the notation $\Omega_M\equiv 8\pi G\rho_0/(3H_0^2)$, which is the ratio of the current matter density to the critical density; $\Omega_k = k/H_0^2$, which gives the global curvature; and $\Omega_\Lambda=\Lambda/(3H_0^2)$, where Λ is the cosmological constant, so that $\Omega_M+\Omega_k+\Omega_\Lambda=1$:

$$H^2(z)=H_0^2[\Omega_M(1+z)^3+\Omega_k(1+z)^2+\Omega_\Lambda]\,. \tag{13}$$

We can now substitute equation (12) into equation (10). In a matter-dominated regime, and for a shear free, nonrotating cosmic fluid, we obtain

$$\frac{d\Theta}{dt}+\frac{1}{3}\Theta^2=-4\pi G\rho+\Lambda\,. \tag{14}$$

On making use of equation (11), we can split Θ as

$$\Theta\equiv\nabla_\mu u^\mu=\frac{3\dot a}{a}+\frac{\theta}{a}\,, \tag{15}$$

so that, taking into consideration the field equations for the expansion factor $a(t)$ (eqs. [5] and [6]), equation (14) can be recast in the form

$$\frac{d\theta}{d\tau}+\mathscr{H}(\tau)\theta+\frac{1}{3}\theta^2=-4\pi G a^2\bar\rho\delta\,, \tag{16}$$

where $\mathscr{H}(\tau)\equiv d(\ln a)/d\tau$. We can now eliminate θ between equations (9) and (16) to find the following second-order differential equation for the density contrast:

$$\frac{d^2\delta}{d\tau^2}+\mathscr{H}(\tau)\frac{d\delta}{d\tau}-\frac{3}{2}\mathscr{H}^2(\tau)\Omega_M(\tau)\delta = \frac{4}{3}(1+\delta)^{-1}\left(\frac{d\delta}{d\tau}\right)^2+\frac{3}{2}\mathscr{H}^2(\tau)\Omega_M(\tau)\delta^2\,, \tag{17}$$

where we have shifted all nonlinear terms to the right-hand side, and have used the notation

$$\Omega_M(\tau)=\frac{\Omega_M}{\Omega_M+a\Omega_k+a^3\Omega_\Lambda}\,. \tag{18}$$

Equation (17) reproduces the equation of the spherical collapse model (SC). In other words, *the SC approximation is the exact dynamics when shear is neglected* (see Fosalba & Gaztañaga 1998a). As one would expect, this yields a *local* evolution, in the sense that the evolved field at a point is just given by a local (nonlinear) transformation of the initial field at the same point, independent of the surroundings. This SC solution yields the exact perturbation-theory predictions for the cumulants at tree level (leading order with Gaussian initial conditions), and it is also an excellent approximation for next-to-leading orders (see below). As mentioned in § 1, one can also use the SC model to predict the value of the critical linear overdensity, δ_c, that will collapse into virialized halos.

2.3. *Linear Growth*

We next do a perturbative expansion for δ. The first contribution is the linear-theory solution. For this, equation (17) clearly simplifies to

$$\frac{d^2\delta_l}{d\tau^2}+\mathscr{H}(\tau)\frac{d\delta_l}{d\tau}-\frac{3}{2}\mathscr{H}^2(\tau)\Omega_M(\tau)\delta_l=0\,, \tag{19}$$

where δ_l stands for the "linear" solution. Because the coefficients of the above equation are time-dependent only, the spatial and temporal part factorize:

$$\delta_l(\boldsymbol{x},\tau)=\delta_0(\boldsymbol{x})D(\tau)\,, \tag{20}$$

where D is usually called the "linear growth factor." Thus, initial fluctuations, no matter what size, are amplified by the same factor, and the statistical properties of the initial field are just linearly scaled. For example, the N-point correlation functions are

$$\xi_N(r_1,\ldots,r_N,t)=D^N\xi_N(r_1,\ldots,r_N,0)\,. \tag{21}$$

To find the solution to equation (19), it is expedient to change the time variable to $\eta=\ln(a)$, so that

$$\frac{d}{d\eta}=\frac{1}{\mathscr{H}(\tau)}\frac{d}{d\tau}=\frac{1}{H}\frac{d}{dt}\,. \tag{22}$$

We then have

$$\frac{d^2D}{d^2\eta}+\left(2+\frac{\dot H}{H^2}\right)\frac{dD}{d\eta}-\frac{3}{2}\Omega_M(\eta)D=0\,, \tag{23}$$

where we can write

$$\frac{\dot H}{H^2}=-\frac{3}{2}\left[\frac{\Omega_M+(2/3)e^\eta\Omega_k}{\Omega_M+e^\eta\Omega_k+e^{3\eta}\Omega_\Lambda}\right], \tag{24}$$

$$\Omega_M(\eta)=\frac{\Omega_M}{\Omega_M+e^\eta\Omega_k+e^{3\eta}\Omega_\Lambda}\,, \tag{25}$$

where Ω_M, Ω_k, and Ω_Λ are just constants (the current value at $a=1$).

In the Einstein–de Sitter universe ($\Omega_k=\Omega_\Lambda=0$), we have $\Omega_M(\eta)=1$ and $\dot H/H^2=-3/2$, so the differential equation becomes

$$\frac{d^2D}{d^2\eta}+\frac{1}{2}\frac{dD}{d\eta}-\frac{3}{2}D=0\,, \tag{26}$$

whose solutions,

$$D=C_1e^\eta+C_2e^{-3/2\eta}=C_1a+C_2a^{-3/2}\,, \tag{27}$$

reproduce the usual linear growth $D\sim a$ and the decaying solutions $D\sim a^{-3/2}$.

2.4. *Nonlinear Growth*

The exact (nonperturbative) solution for the SC equation (17) for the density contrast in an Einstein–de Sitter universe admits a well-known parametric representation:

$$\delta(\varphi) = \frac{9}{2}\frac{(\varphi - \sin\varphi)^2}{(1-\cos\varphi)^3} - 1 ,$$

$$\delta_l(\varphi) = \frac{3}{5}\left[\frac{3}{4}(\varphi - \sin\varphi)\right]^{2/3} , \qquad (28)$$

for $\delta_l > 0$, linear overdensity, and

$$\delta(\varphi) = \frac{9}{2}\frac{(\sinh\varphi - \varphi)^2}{(\cosh\varphi - 1)^3} - 1 ,$$

$$\delta_l(\varphi) = -\frac{3}{5}\left[\frac{3}{4}(\sinh\varphi - \varphi)\right]^{2/3} , \qquad (29)$$

for $\delta_l < 0$, linear underdensity (see Peebles 1993), where the parameter φ is just a parametrization of the time coordinate. There is also a solution for the $\Omega_M \neq 1$ case (see Bernardeau 1992; Fosalba & Gaztañaga 1998b). The continuous line in Figure 1 illustrates the solution to the above equation (the other lines will be explained later). Note the singularity at $\delta_l \simeq 1.686$, which corresponds to gravitational collapse (see § 3.1.3).

If we are only interested in the perturbative regime ($\delta_l \to 0$), which is the relevant one for the description of structure formation on large scales, then the above solution can be expressed directly in terms of the linear density contrast, δ_l, which plays the role of the initial size of the spherical fluctuation in equation (20). This way, the evolved density contrast in the perturbative regime is given by a local-density transformation of the linear density fluctuation,

$$\delta = f(\delta_l) = \sum_{n=1}^{\infty} \frac{v_n}{n!}[\delta_l]^n . \qquad (30)$$

Note that all the nonlinear dynamical information in the SC model is encoded in the v_n coefficients. We can now introduce the above power series expansion in equation (17) and determine the v_n coefficients one by one. Before we do this, it is convenient to again change the time variable to $\eta = \ln(a)$, as we did in the linear case, equation (23):

$$\frac{d^2\delta}{d^2\eta} + \left(2 + \frac{\dot{H}}{H^2}\right)\frac{d\delta}{d\eta} - \frac{3}{2}\Omega_M(\eta)\delta = \frac{4}{3}\frac{1}{1+\delta}\left(\frac{d\delta}{d\eta}\right)^2 + \frac{3}{2}\Omega_M(\eta)\delta^2 . \qquad (31)$$

We can now use the expansion in equation (30) with δ_l given by the linear growth factor $D = a = e^{\eta}$ and compare order by order. For the Einstein–de Sitter universe, they turn out to be

$$v_2 = \tfrac{34}{21} , \quad v_3 = \tfrac{682}{189} , \qquad (32)$$

and so on (see, e.g., Folsalba & Gaztañaga 1998b for other cases). Once we have these coefficients, we can get the evolution of the nonlinear variance and higher order moments in terms of the initial conditions (see § 4.1).

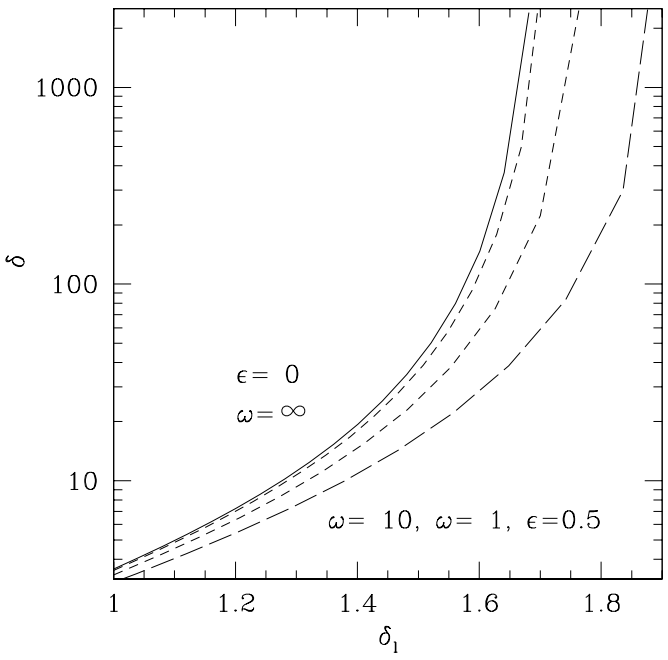

FIG. 1.—Nonlinear density contrast, δ, as a function of the linear one, δ_l, in the spherical collapse. The solid line shows the GR prediction ($\omega = \infty$, $\epsilon = 0$, $\gamma = 0$); the short-dashed lines correspond to the BD model with $\omega = 10$ and $\omega = 1$ (*left to right*). The long-dashed line shows the case with a nonstandard Hubble rate $H^2 = a^{-3(1+\epsilon)}$ for $\epsilon = 0.5$.

2.5. *Equation of State $p = \gamma\rho$*

We now consider a perfect fluid with equation of state $p = \gamma\rho$. Not all values of γ make physical sense. Here, in the spirit of going beyond the standard paradigm, we ignore these restrictions and assume that γ can take any real constant value, irrespective of other cosmological parameters.

The time component of the energy conservation equations $\nabla_\nu T^{\mu\nu} = 0$ gives us (for $p = \gamma\rho$) both the background density behavior,

$$\bar{\rho}a^{3(1+\gamma)} = \text{const} , \qquad (33)$$

and the continuity equation for the density contrast,

$$\frac{d\delta}{d\tau} + (1+\gamma)(1+\delta)\theta = -\gamma\bar{\rho}(\boldsymbol{v}\cdot\nabla\delta), \qquad (34)$$

where, as before, τ is the conformal time, and $\theta \equiv \nabla\cdot\boldsymbol{v}$. This is the generalization of equation (9) for a relativistic fluid. Note that an additional (quadratic) term now appears in the right-hand side of equation (34). The magnitude of this term is assessed by resorting to the space components of the energy conservation equations $\nabla_\nu T^{\mu\nu} = 0$; these are identically satisfied when $\gamma = 0$, and they show that $\boldsymbol{v}\cdot\nabla\delta \propto |\boldsymbol{v}|^2/c^2$, plus higher order contributions. These can be safely neglected, since peculiar velocities are always very small compared to the speed of light; in fact, the approximation $|\boldsymbol{v}|^2/c^2 \to 0$ is always made, even in the more standard case when $\gamma = 0$. We therefore consistently adopt the following equation for the density contrast:

$$\frac{d\delta}{d\tau} + (1+\gamma)(1+\delta)\theta = 0 . \qquad (35)$$

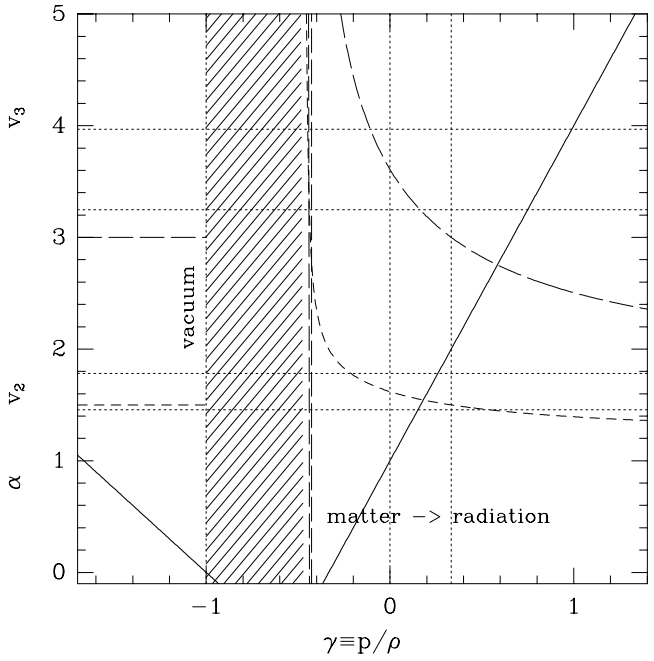

FIG. 2.—Linear growth index α_1 (*solid line*) and nonlinear coefficients v_2 (*short-dashed line*) and v_3 (*long-dashed line*), as a function of $\gamma \equiv p/\rho$. Vertical dotted lines correspond to the vacuum-, matter-, and radiation-dominated cases $\gamma = -1$, 0, and $\frac{1}{3}$. The horizontal dotted lines bracket the v_2 and v_3 regions within 10% error of the matter-dominated ($\gamma = 0$) case.

In addition, Hubble's equation, equation (13), now becomes

$$H^2 = H_0^2[\Omega_M a^{-3(1+\gamma)} + \Omega_k a^{-2} + \Omega_\Lambda] \,. \tag{36}$$

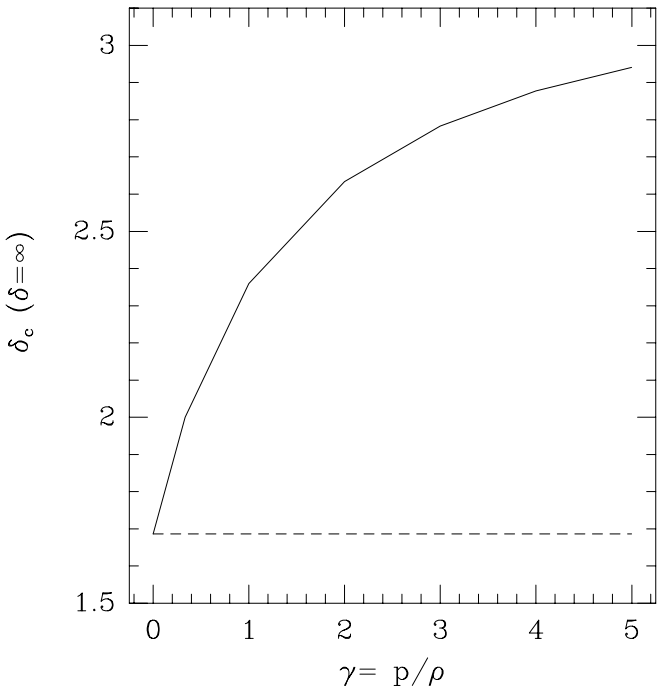

FIG. 3.—Critical value of the linear density contrast, δ_c, where $\delta = \infty$ as a function of $\gamma \equiv p/\rho$.

We can combine equation (35) with the Raychaudhuri equation for this case (cf. eqs. [10] and [12]),

$$\frac{d\Theta}{dt} + \frac{1}{3}\Theta^2 = -4\pi G\rho(1+3\gamma) + \Lambda \,, \tag{37}$$

to obtain, after some algebra,

$$\frac{d^2\delta}{d^2\eta} + \left(2 + \frac{\dot{H}}{H^2}\right)\frac{d\delta}{d\eta} - \frac{3}{2}(1+\gamma)(1+3\gamma)\Omega(\eta)\delta$$

$$= \frac{4+3\gamma}{3+3\gamma}\frac{1}{1+\delta}\left(\frac{d\delta}{d\eta}\right)^2 + \frac{3}{2}(1+\gamma)(1+3\gamma)\Omega(\eta)\delta^2 \,, \tag{38}$$

where we have expediently redefined $\Omega(\eta)$ in equation (25) to

$$\Omega_M(\eta) = \frac{\Omega_M}{\Omega_M + e^{\eta(1+3\gamma)}\Omega_k + e^{3\eta(1+\gamma)}\Omega_\Lambda} \,, \tag{39}$$

and we can write

$$\frac{\dot{H}}{H^2} = -\frac{3}{2}\left[\frac{(1+\gamma)\Omega_M e^{-3\eta\gamma} + (2/3)e^{\eta}\Omega_k}{\Omega_M e^{-3\eta\gamma} + e^{\eta}\Omega_k + e^{3\eta}\Omega_\Lambda}\right] . \tag{40}$$

In an Einstein–de Sitter universe ($\Omega_k = \Omega_\Lambda = 0$), $\Omega(\eta) = 1$, and the linear regime is governed by

$$\frac{d^2D}{d^2\eta} + \frac{1-3\gamma}{2}\frac{dD}{d\eta} - \frac{3}{2}(1+\gamma)(1+3\gamma)D = 0 \,, \tag{41}$$

which has the usual solutions of the form $D = a^\alpha$, with

$$\alpha_1 = 1 + 3\gamma \,, \quad \alpha_2 = -3(1+\gamma)/2 \,. \tag{42}$$

Figure 2 shows these perturbative solutions. The shaded region corresponds to the case in which linear evolution is suppressed, e.g., $\alpha < 0$. In this case, as can be seen from equations (43)–(48), v_2 and v_3 have a very rapid variation. The growing mode for $\gamma > -\frac{1}{3}$ is

$$\alpha_1 = 1 + 3\gamma \,, \tag{43}$$

$$v_2 = \frac{2(17 + 48\gamma + 27\gamma^2)}{3(1+\gamma)(7+15\gamma)} \,, \tag{44}$$

$$v_3 = \left[72 + 540\gamma + 324\gamma^2 + \frac{16}{(1+\gamma)^2} + \frac{24}{1+\gamma} - \frac{(6+18\gamma)(17+48\gamma+27\gamma^2)}{(1+\gamma)(7+15\gamma)}\right] \times (27 + 144\gamma + 189\gamma^2)^{-1} \,. \tag{45}$$

For $\gamma < -1$ the dominant linear growth is α_2, and the values of v_2 and v_3 are constant:

$$\alpha_2 = \frac{-3(1+\gamma)}{2} \,, \tag{46}$$

$$v_2 = \tfrac{3}{2} \,, \tag{47}$$

$$v_3 = 3 \,. \tag{48}$$

For radiation ($\gamma = \frac{1}{3}$), we have $\alpha_1 = 2$, which reproduces the well-known results (see Peebles 1993), and $v_2 = 3/2$ and

$v_3 = 3$, which are new results as far as we know. Note that these values are identical to the case of negative pressure, $\gamma < -1$, the only difference being in the linear growth, but for $\gamma = -7/3$ all α, v_2, and v_3 are identical to the radiation case. In the limit of strong pressure, $\gamma \to \infty$, we find $v_2 = 6/5$ and $v_3 = 12/7$. As can be seen in Figure 2, and also in the equations above, there are poles for v_2 at $\gamma = -1$ and $\gamma = -7/15$.

Figure 3 shows the corresponding variation in δ_c, defined as the value of the linear overdensity where the corresponding nonlinear value becomes infinity (see § 3.1.3).

3. GRAVITATIONAL GROWTH OUTSIDE GR

3.1. *Scalar-Tensor Theories*

Here we investigate how a varying G could change the above results. We parameterize the variation of G using scalar-tensor theories (STT) of gravity, such as the Brans-Dicke (BD) theory or its extensions.

To make quantitative predictions, we consider cosmic evolution in STTs, where G is derived from a scalar field ϕ, which is characterized by a function $\omega = \omega(\phi)$ determining the strength of the coupling between the scalar field and gravity. In the simplest BD models, ω is just a constant, and $G \simeq \phi^{-1}$ (see below). However, if ω varies then it can change with cosmic time, so that $\omega = \omega(z)$. The structure of the solutions to BD equations is quite rich and depends crucially on the coupling function $\omega(\phi)$ (see Barrow & Parsons 1997).

Here we consider the standard BD model with constant ω; the field equations are (see, e.g., Weinberg 1972)

$$R_{\mu\nu} = -\frac{8\pi}{\phi}\left(T_{\mu\nu} - \frac{1+\omega}{3+2\omega}\, g_{\mu\nu} T\right) - \frac{\omega}{\phi^2}\nabla_\mu\phi\nabla_\nu\phi - \frac{1}{\phi}\nabla_\mu\nabla_\nu\phi\phi\,, \tag{49}$$

$$\Box\phi = \frac{8\pi}{3+2\omega}\, T, \qquad (T \equiv g^{\mu\nu}T_{\mu\nu})\,. \tag{50}$$

The Hubble rate, H, for a homogeneous and isotropic background universe can be easily obtained from the above equations:

$$H^2 \equiv \left(\frac{\dot a}{a}\right)^2 = \frac{8\pi\rho}{3\phi} + \frac{k}{a^2} + \frac{\Lambda}{3} + \frac{\omega}{6}\frac{\dot\phi^2}{\phi^2} - H\frac{\dot\phi}{\phi}\,. \tag{51}$$

These equations must be complemented with the equation of state for the cosmic fluid. In a flat, matter-dominated universe ($p = 0$), an exact solution to the problem can be found:

$$G = \frac{4+2\omega}{3+2\omega}\,\phi^{-1} = G_0(1+z)^{1/(1+\omega)} \tag{52}$$

and

$$a(t) = (t/t_0)^{(2\omega+2)/(3\omega+4)}\,. \tag{53}$$

This solution for the flat universe is recovered in a general case in the limit $t \to \infty$, and also arises as an exact solution of Newtonian gravity with a power law $G \propto t^n$ (Barrow 1996). For nonflat models, $a(t)$ is not a simple power law, and the solutions get far more complicated. To illustrate the effects of a nonflat cosmology, we consider general solutions that can be parametrized as equation (52), but which are not simple power laws in $a(t)$. In this case, it is easy to check that the new Hubble law given by equation (51) becomes

$$H^2 = H_0^2[\hat\Omega_M(1+z)^{3+1/(1+\omega)} + \hat\Omega_k(1+z)^2 + \hat\Omega_\Lambda] \tag{54}$$

where $\hat\Omega_M$, $\hat\Omega_k$, and $\hat\Omega_\Lambda$ follow the usual relation $\hat\Omega_M + \hat\Omega_k + \hat\Omega_\Lambda = 1$, and are related to the familiar local ratios [$z \to 0$:$\Omega_M \equiv 8\pi G_0\rho_0/(3H_0^2)$, $\Omega_k = k/H_0^2$, and $\Omega_\Lambda = \Lambda/(3H_0^2)$] by

$$\hat\Omega_M = \Omega_M\frac{3(1+\omega)^2}{(2+\omega)(4+3\omega)}\,,$$

$$\hat\Omega_\Lambda = \Omega_\Lambda\frac{6(1+\omega)^2}{(3+2\omega)(4+3\omega)}\,,$$

$$\hat\Omega_k = \Omega_k\frac{6(1+\omega)^2}{(3+2\omega)(4+3\omega)}\,. \tag{55}$$

Thus, the GR limit is recovered as $\omega \to \infty$.

We now investigate the density fluctuations in the above theory. As in § 2, we make use of the continuity equation (9) in combination with the Raychaudhuri equation (10). As mentioned above (§ 2.1), both of these are still valid within the context of BD theory; it is only necessary to replace the Ricci tensor in the right-hand side of equation (10) according to BD's field equations, equation (49). Considering again a nonrotating, shear-free cosmic fluid, we find

$$\frac{d\Theta}{dt} + \frac{1}{3}\Theta^2 = -\frac{4+2\omega}{3+2\omega}\frac{4\pi\rho}{\phi}\left(1 + \frac{1+\omega}{2+\omega}\frac{3p}{\rho}\right) - \omega\frac{\dot\phi^2}{\phi^2} - \frac{\ddot\phi}{\phi}\,. \tag{56}$$

We still make use of a gravitational "constant" parametrized as in equation (52); this is justified insofar as the characteristic length for the variation of ϕ is typically much greater than that of the density fluctuations in a matter-dominated universe (see, e.g., Nariai 1969). In this approximation, the above equation gives

$$\frac{d\theta}{d\tau} + \mathscr{H}(\tau)\theta + \frac{1}{3}\theta^2 = -\frac{4+2\omega}{3+2\omega}\frac{4\pi a^2\bar\rho\delta}{\phi}\,, \tag{57}$$

where τ is again the conformal time parameter, $d\tau = a^{-1}dt$, and θ is defined in equations (9) and (15). Remarkably, this equation is very similar to the GR equation (4): we only need to replace the gravitational constant G by its expression as a multiple of the varying scalar field ϕ given in equation (52). Combining equation (57) with the continuity equation (9), we immediately find

$$\frac{d^2\delta}{d\tau^2} + \mathscr{H}(\tau)\frac{d\delta}{d\tau} - \frac{4}{3(1+\delta)}\left(\frac{d\delta}{d\tau}\right)^2 = \frac{4+2\omega}{3+2\omega}\frac{4\pi a^2\rho\delta}{\phi}\,. \tag{58}$$

As in § 2, we change the independent variable in equation (58) to $\eta = \ln a$, whereby we obtain

$$\frac{d^2\delta}{d\eta^2} + \left(2 + \frac{\dot H}{H^2}\right)\frac{d\delta}{d\eta} - \frac{4}{3}(1+\delta)^{-1}\left(\frac{d\delta}{d\eta}\right)^2 = \frac{4+2\omega}{3+2\omega}\frac{4\pi a^2\rho\delta}{H^2\phi}\,. \tag{59}$$

Using equation (51) to calculate $\dot{H}$, and assuming further that $\hat{\Omega}_k = \hat{\Omega}_\Lambda = 0$, we finally get

$$\frac{d^2\delta}{d^2\eta} + \frac{1}{2}\frac{\omega}{1+\omega}\frac{d\delta}{d\eta} - \frac{1}{2}\frac{(2+\omega)(4+3\omega)}{(1+\omega)^2}\delta = \frac{4}{3}\frac{1}{1+\delta}\left(\frac{d\delta}{d\eta}\right)^2 + \frac{1}{2}\frac{(2+\omega)(4+3\omega)}{(1+\omega)^2}\delta^2 . \quad (60)$$

We next examine the solutions to this equation.

3.1.1. *Linear Growth*

Let us call $D(\eta)$ the solution to the linearized version of equation (60), i.e.,

$$\frac{d^2D}{d^2\eta} + \frac{1}{2}\frac{\omega}{1+\omega}\frac{dD}{d\eta} - \frac{1}{2}\frac{(2+\omega)(4+3\omega)}{(1+\omega)^2}D = 0 . \quad (61)$$

Again, the solutions are given by the roots α_1 and α_1 of the corresponding characteristic functions:

$$D = C_1 a^{\alpha_1} + C_2 a^{\alpha_2} , \quad (62)$$

where

$$\alpha_1 = \frac{2+\omega}{1+\omega} \simeq 1 + \frac{1}{\omega} + O\left(\frac{1}{\omega^2}\right), \quad (63)$$

$$\alpha_2 = \frac{-4-3\omega}{2+2\omega} \simeq -\frac{3}{2} - \frac{1}{2}\frac{1}{\omega} + O\left(\frac{1}{\omega^2}\right), \quad (64)$$

which reproduces the usual linear growth $D \sim a$ and $D \sim a^{-3/2}$ in the limit $\omega \to \infty$. Note that α_1 corresponds to the growing mode only for large values of $|\omega|$, but the situation is more complicated when ω is not large.

Figure 4 shows the values of α_1 and α_2 as functions of ω. The effective G in BD decreases as the universe expands if $-1 < \omega < \infty$, and the expansion factor $a(t)$ stops for $\omega = -1$; the growing mode in this regime is controlled by α_1, since this is the positive root. The growing mode for $-4/3 < \omega < -1$ is α_2, but the universe shrinks to an eventual collapse in this regime (see eq. [53]). In the range $-2 < \omega < -4/3$ the universe expands again, but there are no growing modes, as can be seen in Figure 4 (both α_1 and α_2 are negative). For $\omega < -2$ the expansion factor grows with time, and α_1 becomes the growing mode again. Note that in this regime of $\omega < -2$, $\alpha_1 < 1$, so that it is slower than for $\omega > 0$. As we show below, this is compensated for in part by a stronger nonlinear growth.

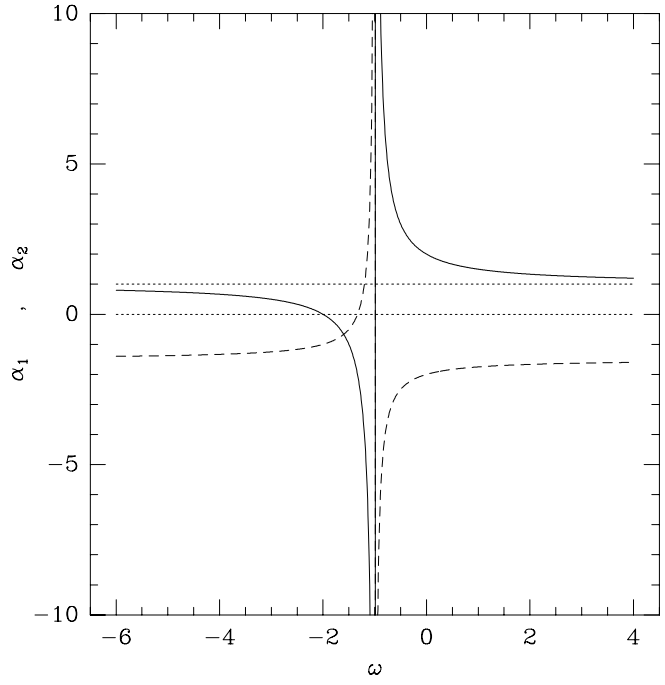

FIG. 4.—Linear growth indices α_1 (*solid line*) and α_2 (*dashed line*), defined by the solution $D = C_1 a_1^{\alpha} + C_2 a_1^{\alpha}$ as a function of the BD parameter ω for a time-varying gravitational constant $G = G_0 a^{-1/(1+\omega)}$.

3.1.2. *Nonlinear Growth*

In the nonlinear case, we consider the full version of equation (60). We can now proceed as before, using the expansion in equation (30) with δ_l given by the linear growth factor $D = a^{\alpha_1} = e^{\alpha_1 \eta}$, and compare order by order. We find

$$v_2 = \frac{34\omega + 56}{21\omega + 36} = \frac{34}{21}\left[1 - \frac{8}{119}\frac{1}{\omega} + O\left(\frac{1}{\omega^2}\right)\right], \quad (65)$$

$$v_3 = \frac{2(944 + 1136\omega + 341\omega^2)}{3(12+7\omega)(16+9\omega)} = \frac{682}{189}\left[1 + \frac{3452}{21483}\frac{1}{\omega} + O\left(\frac{1}{\omega^2}\right)\right]. \quad (66)$$

Note how for positive ω nonlinear effects tend to compensate for the increase in linear effects (cf. Fig. 4), whereas for $\omega < -4/3$ the linear effects are reduced ($\alpha < 1$) while nonlinearities get larger.

Figure 5 shows the variation in v_2 as a function of ω using equation (65). Negative values of ω produce almost symmetrical variations in the opposite direction when $|\omega|$ is large. For small ω there is a pole at $\omega = -12/7$ where v_2 diverges. However, note that there is no growing linear mode in this case, which means that fluctuations are rapidly suppressed.

3.1.3. *Strongly Nonlinear Regime*

Figure 1 shows the fully nonlinear solution for the overdensity, δ, as a function of the linear one, δ_l. The solid line shows the standard solution to equation (17) as given in equations (28) and (29). As can be seen in the figure, there is a critical value of $\delta_l = 3/2(3\pi/2)^{3/2} \simeq 1.6865$ where the nonlinear fluctuations become infinite. This corresponds to the point at which spherical collapse occurs (see Peebles 1993). Thus, an initial fluctuation δ_0 will collapse after evolving a time t, such that the growth factor is $D(t) = \delta_c/\delta_0$. For the standard GR, flat, and matter-dominated case, this time would correspond to a formation redshift $z_f = \delta_0/\delta_c - 1$ (if we use $a = 1$ today). For the BD case, both δ_c and $D(t)$ are different, so that formation times z_f will be correspondingly different (see eq. [87]). The short-dashed lines in Figure 1 correspond to the same exact solution in the BD model with $\omega = 10$ and $\omega = 1$. The right panel in Figure 5 illustrates how δ_c changes in the BD model as a function of ω.

3.2. *Gravitational Growth with $H^2 \sim a^{-3(1+\epsilon)}$*

Consider now the flat case with $\Omega_k = \Omega_\Lambda = 0$. To account for a simple variation on the standard Einstein field equations, we consider the case in which fluctuations grow according to the matter-dominated case (i.e., $\gamma = 0$), but the background evolves in a different way. We assume that the Hubble rate scales as $H^2 \sim a^{-3(1+\epsilon)}$ rather than $H^2 \sim a^{-3}$.

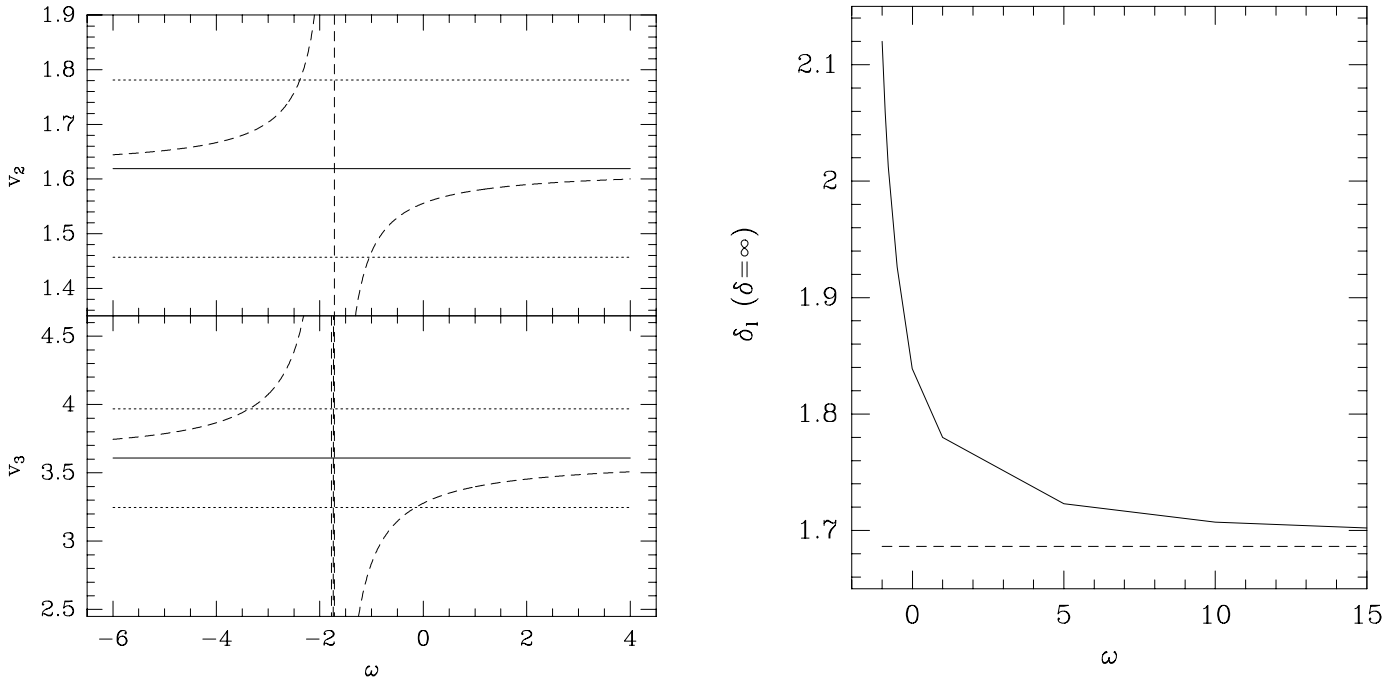

FIG. 5.—*Left*: Dashed lines show v_2 (*top*) and v_3 (*bottom*) as a function of ω for a time-varying gravitational constant $G = G_0\, a^{-1/(1+\omega)}$. The GR results, $G = G_0$ (*solid horizontal lines*) are bracket by 10% errors (*dotted lines*). *Right*: Critical value of the linear density contrast, δ_c, where $\delta = \infty$ as a function of ω.

It might be possible to find some motivation for this model, but this is beyond the scope of this work. Here we just want to introduce some parametric variations around the standard field equations to see how things might change. In this case, we have

$$\frac{d^2\delta}{d^2\eta} + \frac{1-3\epsilon}{2}\frac{d\delta}{d\eta} - \frac{3}{2}\delta = \frac{4}{3}\frac{1}{1+\delta}\left(\frac{d\delta}{d\eta}\right)^2 + \frac{3}{2}\delta^2 \,. \quad (67)$$

The solutions for the linear growth factor index and the nonlinear coefficient v_2 are

$$\alpha_1 = \frac{-1 + 3\epsilon + \sqrt{25 - 6\epsilon + 9\epsilon^2}}{4}\,, \quad (68)$$

$$v_2 = \frac{131 - 30\epsilon + 45\epsilon^2 + (1-3\epsilon)\sqrt{25 - 6\epsilon + 9\epsilon^2}}{84 - 18\epsilon + 27\epsilon^2}\,. \quad (69)$$

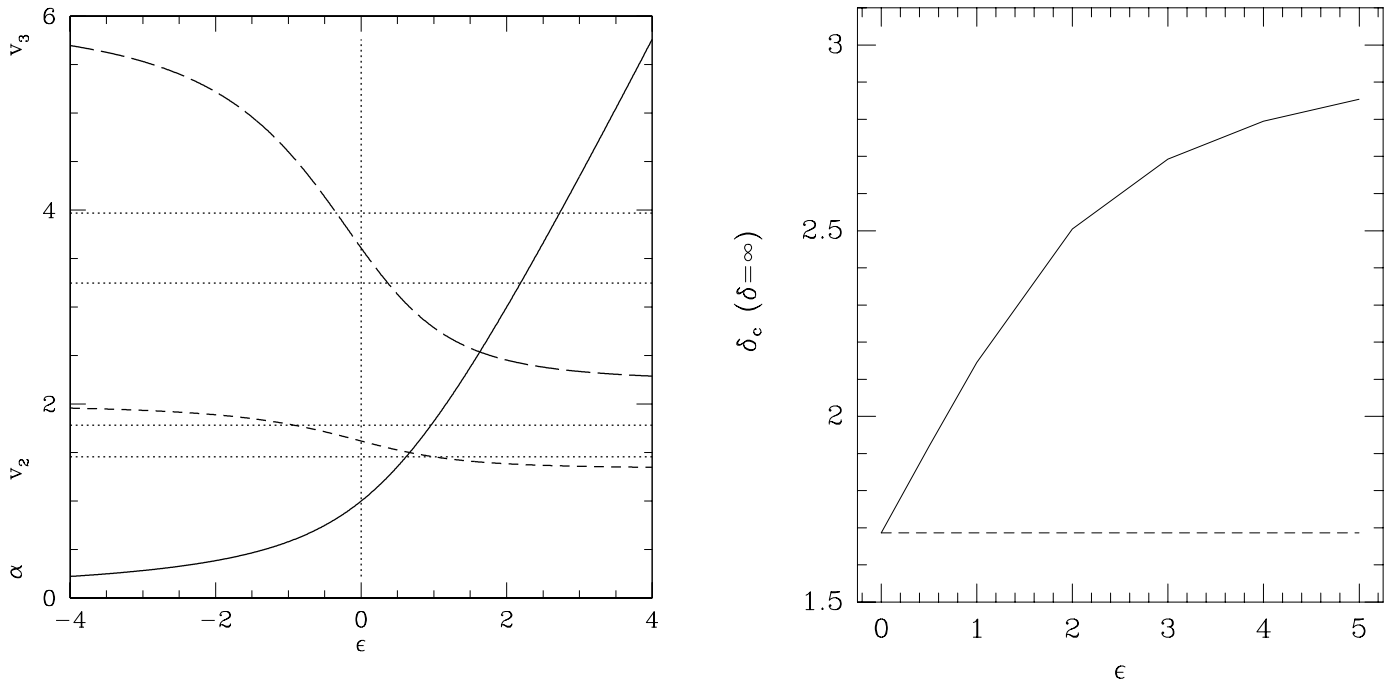

FIG. 6.—*Left*: Linear growth index α_1 (*solid line*) and nonlinear coefficients v_2 (*short-dashed line*) and v_3 (*long-dashed line*), as a function of ϵ, which parameterizes a nonstandard Hubble rate $H^2 \sim a^{-3(1+\epsilon)}$. Vertical dotted line corresponds to the standard Hubble law ($\epsilon = 0$). The horizontal dotted lines bracket the v_2 and v_3 regions within 10% error of the standard ($\epsilon = 0$) case. *Right*: Critical value of the linear density contrast, δ_c, where $\delta = \infty$ as a function of ϵ.

These solutions as a function of ϵ are illustrated in Figure 6, which also shows v_3. As can be seen in the figure, the higher the linear growth index α_1, the lower the nonlinear coefficients. The right panel in Figure 6 shows the corresponding variation in δ_c.

4. OBSERVATIONAL CONSEQUENCES

We focus here on Gaussian initial conditions. That is, our initial field for structure formation is a spatial realization of a (three-dimensional) Gaussian distribution with a given power-spectrum shape and a very small initial amplitude. Since we are interested in the gravitational regime alone, this field will be smoothed over a large enough scale, corresponding to the distance beyond which nongravitational forces (e.g., hydrodynamics) can be neglected. Thus, at each point the overdensity $\delta(\boldsymbol{x})$ grows according to gravity, which in the shear-free approximation is just a local dynamics: the spherical collapse (e.g., eq. [17]).

4.1. *Cumulants*

Consider the J-order moments of the fluctuating field,

$$m_J \equiv \langle \delta^J \rangle \, . \tag{70}$$

Here the expectation values $\langle \dots \rangle$ correspond to an average over realizations of the initial field. On comparing with observations, we assume the "fair sample hypothesis" (see § 30 of Peebles 1980), by which we can commute spatial integrals with expectation values. Thus, in practice $\langle \dots \rangle$ is the average over positions in the survey area. In this notation, the variance is defined as

$$\mathrm{Var}\,(\delta) \equiv \sigma^2 \equiv m_2 - m_1^2 \, . \tag{71}$$

More generally, we introduce the "connected moments" $\overline{\xi}_J$, which carry statistical information independent of the lower order moments, and are formally denoted by a bracket with subscript c:

$$\overline{\xi}_J \equiv \langle \delta^J \rangle_c \, . \tag{72}$$

The connected moments are also called cumulants, reduced moments, or irreducible moments. They are defined by just subtracting the lower order contributions:

$$\begin{aligned}
&\overline{\xi}_1 = m_1 \equiv 0 \, , \\
&\overline{\xi}_2 = \sigma^2 = m_2 - \overline{\xi}_1^2 = m_2 \, , \\
&\overline{\xi}_3 = m_3 - 3\overline{\xi}_2\,\overline{\xi}_1 - \overline{\xi}_1^3 = m_3 \, , \\
&\overline{\xi}_4 = m_4 - 4\overline{\xi}_3\,\overline{\xi}_1 - 3\overline{\xi}_2^2 - 6\overline{\xi}_2\,\overline{\xi}_1^2 - \overline{\xi}_1^4 = m_4 - 3m_2^2 \, ,
\end{aligned} \tag{73}$$

and so on. It is useful to introduce the "hierarchical ratios":

$$S_J = \frac{\overline{\xi}_J}{\overline{\xi}_2^{J-1}} \, , \tag{74}$$

which are also called normalized one-point cumulants or reduced cumulants. We use the term "skewness" for $S_3 = \overline{\xi}_3/\overline{\xi}_2^2$ and "kurtosis" for $S_4 = \overline{\xi}_4/\overline{\xi}_2^3$.

4.1.1. *Linear Theory*

As mentioned in § 2.3, initial fluctuations, δ_0, no matter of what amplitude, all grow by the same factor, D; thus, the statistical properties of the initial field are just linearly scaled in the final (linear) field, δ_l:

$$\langle \delta_l^J \rangle_c = D^J \langle \delta_0^J \rangle_c \, . \tag{75}$$

Consider, for example, the linear rms fluctuations σ_l or its variance σ_l^2. In the linear regime, we have

$$\sigma_l^2 \equiv \langle \delta^2(t) \rangle = \langle D(t - t_0)^2 \delta_0^2 \rangle = D(t - t_0)^2 \sigma_0^2 \, , \tag{76}$$

where σ_0 refers to some initial reference time t_0. To give an idea of this effect, consider the growth of fluctuations since matter domination, when the universe was about 1100 times smaller. In GR, in the matter-dominated Einstein–de Sitter universe, σ would grow by a factor $D \simeq 1100$. However, if we take $\omega \simeq 10$ in the DB theory (e.g., eq. [63]), we find that fluctuations increase instead by a factor $D \simeq 2079$, which is about 1.9 times larger in σ, so the variance nowadays would be about 3.6 times larger if we fixed it around the *COBE* variance of the cosmic microwave background (CBM) temperature fluctuations. For $\omega \simeq 100$, the variance would only be 14% larger than in GR. This latter result is small, but it could be relevant for future precision measurements (e.g., *MAP* or *Planck* satellites to map CMB, and Two-Degree Field [2DF] or Sloan Digital Sky Survey [SDSS] galaxy surveys). Similar considerations can be made for the values of α with a different cosmic equation of state (e.g., eq. [43]) or a different Hubble law (eq. [68]). In general, we can write that a small change in α would produce a relative change in the linear rms of

$$\frac{\Delta\sigma}{\sigma} = \ln(1 + z)\Delta\alpha \, . \tag{77}$$

Thus, a change of only 1% in the absolute value of the equation of state γ would produce a relative change of 20% in σ between recombination ($z \simeq 1100$) and now (cf. eq. [43]).

The hierarchical ratios (see eq. [74]) will scale as $S_J = S_J(0)/D^{J-2}$, where $S_J(0)$ are the initial ratios. This implies that the linear growth erases the initial skewness and kurtosis, so that $S_J \to 0$ as time evolves (and $D \to \infty$). Note that if we want to do a meaningful calculation of these ratios or the cumulants, in general we might need to consider more terms in the perturbative series, equation (30). For Gaussian initial conditions $S_J(0) = 0$, and we need to consider higher order terms in the perturbation series to find the leading-order prediction.

4.1.2. *Weakly Nonlinear*

The next-to-leading-order solutions for the cumulants of the evolved field, given the expansion equation (30), can be easily found by just taking expectation values of different powers of δ (see, e.g., Fosalba & Gaztañaga 1998a). For leading-order Gaussian initial conditions, we have

$$\begin{aligned}
S_3 &= 3v_2 + O(\sigma_l^2) \, , \\
S_4 &= 4v_3 + 12v_2^2 + O(\sigma_l^2) \, .
\end{aligned} \tag{78}$$

For non-Gaussian initial conditions, see Fry & Scherrer (1994), , Chodorowski & Bouchet (1996), Gaztañaga & Mahonen (1996), and Gaztañaga & Fosalba (1998).

If we use for v_2 the solution in equation (32), e.g., $v_2 = 34/21$, the skewness yields $S_3 = 3v_2 = 34/7$, which reproduces the exact perturbation-theory (PT) result by Peebles (1980) in the matter-dominated Einstein–de Sitter universe. Thus, the shear-free or SC model gives the exact leading-order result for the skewness. This is also true for higher orders (see Bernardeau 1992; Fosalba & Gaztañaga 1998a) and for other cosmologies (e.g., Bouchet, Juszkiewicz, &

Colombi 1992; Bernardeau 1994a; Fosalba & Gaztañaga 1998b; Kamionkowski & Buchalter 1999). For smoothed fields, the exact leading-order results are slightly different:

$$S_3 = \tfrac{34}{7} + \gamma_1 ,$$
$$S_4 = \tfrac{60712}{1323} + \tfrac{62}{3}\,\gamma_1 + \tfrac{7}{3}\,\gamma_1^2 , \qquad (79)$$

where γ_1 is the logarithmic slope of the smoothed variance (see Juszkiewicz, Bouchet, & Colombi 1993; Bernardeau 1994a, 1994b). These can also be reproduced in the shear-free approximation, as shown by Gaztañaga & Fosalba (1998); this results in a smoothing correction

$$\overline{v_2} = v_2 + \frac{\gamma_1}{3} ,$$
$$\overline{v_3} = \tfrac{1}{4}(-2\gamma_1 + \gamma_1^2 + 6\gamma_1 v_2 + 4v_3), \qquad (80)$$

and replacing v_2 and v_3 by $\overline{v_2}$ and $\overline{v_3}$ in equation (78) (see Fosalba & Gaztañaga 1998a for more details). There are also corrections to the above expressions when measurements are taken in redshift space (e.g., Hivon et al. 1995; Scoccimarro, Couchman, & Frieman 1999). Next-to-leading-order terms have been estimated by Scoccimarro & Frieman (1996; see also Fosalba & Gaztañaga 1998a, 1998b).

The smoothed values of S_3 and S_4 can be measured as traced by the large-scale galaxy distribution (e.g., Bouchet et al. 1993; Gaztañaga 1992, 1994; Szapudi el at 1995; Hui & Gaztañaga 1999, and references therein), weak lensing (Bernardeau, van Waerbeke, & Mellier 1997; Gaztañaga & Bernardeau 1998; Hui 1999), or the Lyα QSO absorptions (Gaztañaga & Croft 1999). These measurements of the skewness and kurtosis can be translated into estimations of v_2 and v_3 that can be used to place constraints on γ, ω, or ϵ using equations (44), (65), and (69). For small values of these parameters the relationship is linear, so the uncertainties in S_3 and S_4 would directly translate into the corresponding uncertainties in γ, ω, or ϵ.

The expressions above apply to unbiased tracers of the density field; since galaxies of different morphologies are known to have different clustering properties, at least some galaxy species must be biased tracers of the mass. As an example, suppose the probability of forming a luminous galaxy depends only on the underlying mean density field in its immediate vicinity. Under this simplifying assumption, the relation between the galaxy density field, $\delta_{\rm gal}(\boldsymbol{x})$, and the mass density field, $\delta(\boldsymbol{x})$, can be written as

$$\delta_{\rm gal}(\boldsymbol{x}) = f(\delta(\boldsymbol{x})) = \sum_n \frac{b_n}{n!}\,\delta^n(\boldsymbol{x}) , \qquad (81)$$

where b_n are the bias parameters. Thus, biasing and gravity could produce comparable nonlinear effects. To leading order in $\overline{\xi}_2$, this local bias scheme implies $\overline{\xi}_2^{\rm gal} = b_1^2\,\overline{\xi}_2$, and (see Fry & Gaztañaga 1993)

$$S_3^{\rm gal} = \frac{S_3}{b_1} + 3\,\frac{b_2}{b_1^2} ,$$
$$S_4^{\rm gal} = \frac{S_4}{b_1^2} + 12\,\frac{b_2 S_3}{b_1^3} + 4\,\frac{b_3}{b_1^4} + 12\,\frac{b_2^2}{b_1^4} . \qquad (82)$$

Gaztañaga & Frieman (1994) have used the comparison of S_3 and S_4 in PT with the corresponding values measured by the Automated Plate Measuring Facility (APM) Galaxy Survey (Maddox et al. 1990), to infer that $b_1 \simeq 1$, $b_2 \simeq 0$, and $b_3 \simeq 0$, but the results are degenerate due to the relative scale-independence of S_N and the increasing number of biasing parameters. One could break this degeneracy by using the configuration dependence of the projected three-point function, $q_3(\alpha)$, as proposed by Frieman & Gaztañaga (1994), Fry (1994), Matarrese, Verde, & Heavens (1997), and Scoccimarro et al. (1998). As shown in Frieman & Gaztañaga (1999), the configuration dependence of $q_3(\alpha)$ on large scales in the APM catalog is quite close to that expected in perturbation theory (see Fry 1984; Scoccimarro et al. 1998; Buchalter, Jaffe, & Kamionkowski 2000), suggesting again that b_1 is of order unity (and $b_2 \simeq 0$) for these galaxies. These agreement indicates that large-scale structure is driven by nonlinear gravitational instability and that APM galaxies are relatively unbiased tracers of the mass on these large scales.

The values of S_3 and S_4 in the APM are measured to agree with the standard matter-dominated Einstein–de Sitter universe within about 10%–20% (see Gaztañaga 1994, 1995; Gaztañaga & Frieman 1994; Baugh et al. 1995; Hui & Gaztañaga 1999), and are also in agreement with the shape information in the three-point function (see Frieman & Gaztañaga 1999). For example, using the projected APM catalog, Gaztañaga (1994, Table 3) finds an average of $S_3 = 3.2 \pm 0.2$ and $S_4 \pm 20.6 \pm 2.6$ scales between 7 and 30 h^{-1} Mpc. For an average APM slope of $\gamma_1 \simeq 1.7$, these values are in agreement with the PT predictions in equation (79), yielding $S_3 \simeq 3.1$ and $S_4 \simeq 18$.

The 1 σ error bar of $\simeq$10% on large scales quoted by Gaztañaga (1994) is mostly statistical (sampling error). Other systematic effects due to biasing, projection, or large-scale errors in the building of the APM catalog could be of the same order (see Frieman & Gaztañaga 1999; Hui & Gaztañaga 1999). Thus, given the current uncertainties, it would be conservative to take a 20% error bar. Unfortunately, with such large error bars we cannot much constrain the values of γ, ω, or ϵ. Stronger constraints can be found if we take the more optimistic 1 σ 10% error bars in the measurements of S_3 and S_4. This case is shown by horizontal dotted lines in Figures 2, 5, and 6. From v_2, the 10% uncertainty translates into

$$-0.2 < \gamma < 0.4 ,$$
$$-2.4 > \omega > -1.0 ,$$
$$-0.9 < \epsilon < 0.9 . \qquad (83)$$

Note that this is still of marginal interest. For example, the constraints on γ include the possibility of a radiation ($\gamma = \frac{1}{3}$), matter ($\gamma = 0$), or negative pressure $\gamma < 0$. From v_3 we can obtain stronger constraints from a 10% error (but obviously systematic effects could be larger for higher order cumulants):

$$-0.1 < \gamma < 0.15 ,$$
$$-3.4 > \omega > -0.2 ,$$
$$-0.35 < \epsilon < 0.35 . \qquad (84)$$

These bounds are more interesting. It is clear that forthcoming surveys (such as SDSS) will dramatically improve

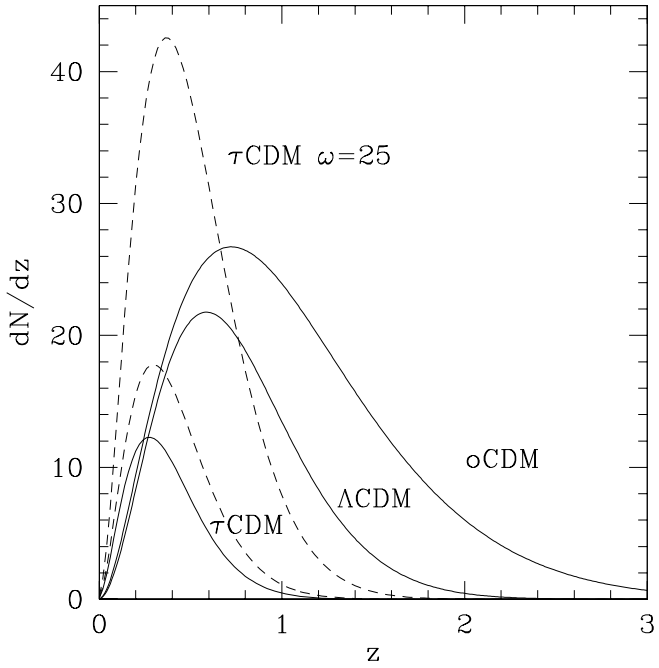

FIG. 7.—Solid lines represent the expected differential count distribution per deg^2 of massive clusters ($M > M_{\rm th} \times 10^{14}\ h_{50}^{-1}\ M_\odot$) for three cosmologies: oCDM ($M_{\rm th} = 1.9$, $\Omega_m = 0.3$, $\Omega_\Lambda = 0$, $h = 0.65$, $\Gamma = 0.25$, $\sigma_8 = 1.0$), ΛCDM ($M_{\rm th} = 2.2$, $\Omega_m = 0.3$, $\Omega_\Lambda = 0.7$, $h = 0.65$, $\Gamma = 0.25$, $\sigma_8 = 1.0$), and τCDM ($M_{\rm th} = 1.3$, $\Omega_m = 1.0$; $\Omega_\Lambda = 0$, $h = 0.5$, $\Gamma = 0.25$, $\sigma_8 = 0.56$), derived using the Press-Schechter prescription. The bottom and top dashed lines correspond to the a Brans-Dicke Cosmology with $\omega = 100$ and 25, respectively, normalized to *COBE* with the τCDM model.
.

this situation (for errors on statistics, see Szapudi, Colombi, & Bernardeau 1999, and references therein).

Note that the above results are independent of the normalization of fluctuations.

4.2. *Collapsed Objects*

Press & Schechter (1974) formalism and its extensions (e.g., Bond et al. 1991; Lacey & Cole 1993) predict the evolution of the mass function of halos and also their clustering properties. Comparison with N-body simulations show a very good agreement of these prescriptions for a wide range of statistical properties (see, e.g., Lacey & Cole 1994, and references therein). For example, the comoving number density of collapsed objects (halos or clusters) of mass M is

$$n(M)dM = -\sqrt{\frac{2}{\pi}}\left(\frac{\delta_c}{\sigma}\right)\frac{d\ln\sigma}{d\ln M}\exp\left(-\frac{\delta_c^2}{2\sigma^2}\right)\frac{\bar{\rho}\,dM}{M^2}, \quad (85)$$

where $\sigma = \sigma(R)$ is the current linear rms fluctuation at the scale R corresponding to the mass $M = 4/3\pi R^3\bar{\rho}$, and $\bar{\rho}$ is the mean background. The value of δ_c corresponds to the value of the linear overdensity at the time of collapse. The collapsing structure virializes when the (nonlinear) overdensity becomes very large ($\delta \gtrsim 100$). The actual definition is not very important, since once $\delta \gtrsim 100$ the nonlinear collapse is quite rapid, as can be seen in the plots of Figure 1, and the corresponding value of δ_l does not change much. Here we take δ_c to be the critical value where $\delta \to \infty$; other prescriptions (e.g., the value of δ_l corresponding $\delta \simeq 178$) yield similar results. For the standard Einstein–de Sitter case, we have $\delta_c \simeq 1.686$. Note that the above abundance depends on the ratio

$$\nu \equiv \frac{\delta_c}{\sigma}. \quad (86)$$

The time of collapse or formation is just given by the ratio of δ_c to the linear overdensity δ_l today,

$$z_f = \left(\frac{\delta_l}{\delta_c}\right)^{1/\alpha} - 1, \quad (87)$$

so that an object that has $\delta_l = \delta_c$ now has a formation redshift $z_f = 0$, while a fluctuation 4 times larger collapses at $z_f = 3$ if $\alpha = 1$, or at $z_f = 1$ if $\alpha = 2$.

Nonstandard parameterization of the spherical collapse considered in the previous sections can change the above formalism in two ways. If we label an object by its *initial* overdensity, δ_0, then the corresponding δ_l today is

$$\delta_l = \delta_0\, a^\alpha. \quad (88)$$

Thus, a different value of α from the standard GR result ($\Delta\alpha \equiv \alpha - \alpha_{\rm GR}$), as shown in Figures 2, 4, and 6, will produce a different amplitude of linear fluctuations today. Moreover, as shown in § 3.1.3 and Figures 3, 5, and 6, the solution to the spherical collapse equation produces different values of δ_c, and therefore different mass functions and formation times. Finally, for a directly measurable quantity, such as the surface density of objects, typically one needs the volume element, which is also a function of the cosmology.

For example, if fluctuations are normalized at a given redshift, z_n, then the change in δ_l today will be

$$\frac{\Delta\delta_l}{\delta_l} = \Delta\alpha\,\log(1 + z_n). \quad (89)$$

For recombination, e.g., *COBE* normalization, we have $z_n \simeq 1100$, and

$$\frac{\Delta\delta_l}{\delta_l} \simeq 3\Delta\alpha. \quad (90)$$

In the case of the BD theory, we can see in Figure 4 that for $\omega > -1$, $\Delta\alpha \equiv \alpha - \alpha_{\rm GR} > 0$, which means that $\Delta\delta_l > 0$. This makes sense, since the linear growth is faster, and, for fixed initial fluctuations, the final linear overdensity will be larger. As shown in right panel of Figure 5, δ_c will also be larger. Thus, in this case the effects tend to compensate for each other. This is true for either the formation redshift z_f or ν in equation (86) above. For the formation redshift z_f, we have

$$\frac{\Delta z_f}{1 + z_f} \simeq \frac{1}{\alpha}\left(\frac{\Delta\delta_l}{\delta_l} - \frac{\Delta\delta_c}{\delta_c}\right), \quad (91)$$

which is only valid for small changes. In the BD example given above with $\omega = 10$ (and *COBE* normalization), we have $\Delta\delta_l/\delta_l \simeq 0.9$ while $\Delta\delta_c/\delta_c \simeq 0.01$, so the net effect is still quite large. In this case, a formation redshift of $z_f = 1$ will change to $z_f = 1.39$. Thus, a positive finite ω (which corresponds to a larger G at high redshifts) tends to produce larger (earlier) formation redshifts and higher densities (or larger abundances) at a given redshift than the standard model. This goes in the direction of some recent observations (see, e.g., Bahcall & Fan 1998; Robinson, Gawiser,

& Silk 1998; Willick 2000), which seem to need larger abundances than expected in some standard cosmologies. This interpretation is degenerate with respect to initial conditions and cosmological parameters.

Figure 7 illustrates the large differences in the cluster counts that can be seen between different cosmological models at $z > 1$ (see Holder et al. 2000 for details). Deviations from GR in the BD models with $\omega = 100$ and 25 can be noticed even at low redshift, when models are normalized to CMB fluctuations.

A similar trend is found for the case of Hubble rate $H^2 = a^{-3(1+\epsilon)}$ parameterization. A change of $|\Delta\epsilon| \simeq 0.3$ (allowed by the bounds in eq. [84]), when normalized to *COBE*, also produces $|\Delta\delta_l/\delta_l| \simeq 0.9$ and a smaller effect on $\Delta\delta_c/\delta_c$. This translates into a similar change (of several tens to hundreds of percent) in z_f. Earlier (or later) formation times and larger (or smaller) abundances are found for $\epsilon > 0$ (or $\epsilon < 0$, respectively).

The change in the equation of state, $p = \gamma\rho$, could produce comparable effects. The allowed values in equation (84) of $|\Delta\gamma| \simeq 0.1$ translate into $|\Delta\delta_l/\delta_l| \simeq 0.3$, which results in similar changes for z_f in either direction, with earlier formation for $\gamma > 0$.

If the normalization is not fixed, i.e., if we do not quite know the value of the initial fluctuation that gave rise to an object we see today (e.g., a cluster), then all the relative change in the formation or abundance comes through δ_c, which tends to produce smaller (later) formation redshifts (δ_c is larger than the standard GR value) and lower densities (or smaller abundances) at a given redshift.

5. DISCUSSION AND CONCLUSIONS

We have reconsidered the problem of nonlinear structure formation in two different contexts that relate to observations: one-point cumulants of large-scale density fluctuations, and the epoch of formation and abundance of structures using the Press & Schechter (1974) formalism. We have use the shear-free or spherical collapse (SC) model, which is a very good approximation for the above applications. We have addressed the question of how different the predictions are when using a nonstandard theory of gravity, such as the BD model, or a nonstandard cosmological model (e.g., a different equation of state or Hubble law). Note that these are slight variations on the standard theme in the sense that they preserve the main ingredients of GR, such as the covariance and the geometrical aspects of the theory, including the same metric, with only slight changes in the field equations.

We have also presented some preliminary bounds on γ, ω, and ϵ from observations of the skewness and kurtosis in the APM Galaxy Survey, e.g., equations (83)–(84). These bounds are optimistic given the current data, but the situation is going to change rapidly, and one can hope to find much better bounds from upcoming data (such as the 2DF or SDSS projects). In terms of the equation of state, the bounds in equation (84) would indicate that our universe is neither radiation ($\gamma = \frac{1}{3}$) nor vacuum dominated ($\gamma = -1$), but somewhere in between (e.g., matter dominated). In terms of the gravitational constant, the bounds on ω from equation (84) would say that G has not changed by more than $\simeq 5\%$ from $z \simeq 1.15$, or by distances of $\simeq 400\ h^{-1}$ Mpc. Clustering at higher redshift would probe much larger scales and times. In terms of ϵ, the bounds equation (84) would say that the Hubble law does not differ by more than 7% from the standard result (assumed here to be $\epsilon = 0$). We have also shown how halo and cluster abundances and formation times could change in these nonstandard cases. The above bounds on γ, ω, and ϵ from observations of the skewness and kurtosis in the APM still allow significant changes (of several tens to hundreds of percent) on formation redshifts z_f and the corresponding abundances (see § 4.2).

In the context of BD models, the limits we find for ω are less restrictive than the solar system limits, $\omega \gtrsim 100$. However, BD models allow $\omega = \omega(\phi)$, so that ω can increase with cosmic time, $\omega = \omega(z)$, in such a way that it could approach the general relativity predictions ($\omega \to \infty$) at the present time and still give significant deviations at earlier cosmological times. It is important to recall that our theory of gravity has only been tested on stellar distances (AU), while we want to use it on cosmological scales (Mpc). Our working example shows, for the first time, how nonlinear effects are changed in such a model, and it sets the framework to study nonlinear effects of more complicated (or realistic) scalar-tensor theories of gravity.

It is straightforward to combine several of the changes proposed here to explore more general situations. One could, for example, parameterize theories in the (γ, ω) plane, e.g., different equations of state with different BD parameters, or consider the whole (γ, ω, Ω_M, Ω_Λ) space. One could also consider a different equation of state for the Λ component, as in quintessence cosmologies (Caldwell, Dave, & Steinhardt 1998); such models have already been used to predict cluster abundances within the "standard" cosmology (see Haiman, Mohr, & Holder 2000, and references therein). This would obviously allow for a wider set of possible solutions and degeneracies. One should also consider other observational consequences of these variations, in particular relating to BD theory, such as the age of the universe, the effects on CMB (see, e.g., Chen & Kamionkowski 1999), radiation-matter transition (Liddle, Mazumdar, & Barrow 1998), or the constraints from nucleosynthesis (Santiago, Kalligas, & Wagoner 1997). These considerations could rule out some aspects of the proposed variations on the standard model, or might require more elaborate solutions [e.g., $\omega = \omega(\phi)$, which implies $\omega = \omega(z)$]. However, even if this were the case, we still have learned a few new things about how structure formation depends on the underlying theory of gravity, which is a first step toward further analysis of these issues.

Throughout this paper we have assumed Gaussian initial conditions and no biasing. Both biasing (e.g., Fry & Gaztañaga 1993) and non-Gaussianities in the initial conditions (Gaztañaga & Fosalba 1998) would provide an additional source of degeneracy, since they might produce similar effects as the nonstandard variations presented here. This is the case, for example, when we have nonzero initial skewness or kurtosis, which could produce quite different values of S_3 and S_4 (see, e.g., Gaztañaga & Mahonen 1996; Peebles 1999a, 1999b; White 1999; Scoccimarro 2000), and therefore inferred values of ν_2 and ν_3. Biasing can have a very similar effect (see, e.g., Mo et al. 1997). One would also expect some level of degeneracy with biasing and initial conditions for cluster abundances or formation times (see Robinson et al. 1998; Willick 2000).

Rather than proposing an alternative theory of gravity or cosmological model, the aim of this paper has been to show that some small deviations from the current paradigm have significant and measurable consequences for nonlinear

structure formation. This could eventually help to explain some of the current puzzles confronting the theory, such as the need for nonbaryonic dark matter. Alternatively, current and upcoming observations of nonlinear clustering and mass functions can be used to explore our assumptions and place limits on the theory of gravity at large ($\gtrsim 1\ h^{-1}$ Mpc) scales. This provides an interesting test for gravity as the driving force for structure formation and for our knowledge of the cosmological equation of state. A more comprehensive comparison with particular scenarios is left for future work.

One of us (J. A. L.) gratefully acknowledges financial support from the Spanish Ministry of Education, contract PB96-0384, and also Institut d'Estudis Catalans. E. G. acknowledges support from CSIC, DGICYT (Spain), project PB96-0925. We would like to thank IEEC, where most of this work was carried out.

REFERENCES

Bahcall, N. A., & Fan, X. 1998, ApJ, 504, 1
Barrow, J. D. 1996, MNRAS, 282, 1397
Barrow, J. D., & Parsons, P. 1997, Phys. Rev. D, 55, 1906
Baugh, C. M., & Gaztañaga, E. 1996, MNRAS, 280, L37
Baugh, C. M., Gaztañaga, E., & Efstathiou, G. 1995, MNRAS, 274, 1049
Bernardeau, F. 1992, ApJ, 392, 1
———. 1994a, A&A, 291, 697
———. 1994b, ApJ, 433, 1
Bernardeau, F., van Waerbeke, L., & Mellier, Y. 1997, A&A, 322, 1
Bond, J. R., Cole, S., Efstathiou, G., & Kaiser N. 1991, ApJ, 379, 440
Bouchet, F. R., Juszkiewicz, R., & Colombi, S. 1992, ApJ, 394, L5
Bouchet, F. R., Strauss, M. A., Davis, M., Fisher, K. B., Yahil, A., & Huchra, J. P. 1993, ApJ, 417, 36
Buchalter, A., Jaffe, A., & Kamionkowski, M. 2000, ApJ, 530, 36
Caldwell, R. R., Dave, R., & Steinhardt, P. J. 1998, Ap&SS, 261, 303
Chen, X., & Kamionkowski, M. 1999, Phys. Rev. D, 60, 104036
Chodorowski, M., & Bouchet, F. 1996, MNRAS, 279, 557
Colombi, S., Bernardeau, F., Bouchet, F. R., & Hernquist, L. 1997, MNRAS, 287, 241
Ellis, G. F. R. 1999, Classical Quantum Gravity, 16, A37
Fosalba, P., & Gaztañaga, E. 1998a, MNRAS, 301, 503
———. 1998b, MNRAS, 301, 535
Frieman, J. A., & Gaztañaga, E. 1994, ApJ, 425, 392
———. 1999, ApJ, 521, L83
Fry, J. N. 1984, ApJ, 279, 499
———. 1994, Phys. Rev. Lett., 73, 215
Fry, J. N., & Gaztañaga, E. 1993, ApJ, 413, 447
Fry, J. N., & Scherrer, R. J. 1994, ApJ, 429, 36
Gaztañaga, E. 1992, ApJ, 398, L17
———. 1994, MNRAS, 268, 913
———. 1995, ApJ, 454, 561
Gaztañaga, E., & Bernardeau, F. 1998, A&A, 331, 829
Gaztañaga, E., & Croft, R. A. C. 1999, MNRAS, 309, 885
Gaztañaga, E., & Fosalba, P. 1998, MNRAS, 301, 524
Gaztañaga, E., & Frieman, J. A. 1994, ApJ, 437, L13
Gaztañaga, E., & Mahonen, P. 1996, ApJ, 462, L1
Haiman, Z., Mohr, J., & Holder, G. 2000, ApJ, submitted (preprint astro-ph/0002336)
Hivon, E., Bouchet, F. R., Colombi, S., & Juszkiewicz, R. 1995, A&A, 298, 643
Holder, G. P., et al. 2000, ApJ, 544, 629
Hui, L. 1999, ApJ, 519, L9
Hui, L., & Gaztañaga, E. 1999, ApJ, 519, 622
Jain, B., & Van Waerbeke, L. 2000, ApJ, 530, L1
Juszkiewicz, R., Bouchet, F. R., & Colombi, S. 1993, ApJ, 412, L9
Kamionkowski, M., & Buchalter, A. 1999, ApJ, 514, 7
Lacey, C., & Cole, S. 1993, MNRAS, 262, 627
———. 1994, MNRAS, 271, 676
Liddle, A. R., Mazumdar, A., & Barrow, J. D. 1998, preprint (astro-ph/9802133)
Maddox, S. J., Efstathiou, G., Sutherland, W. J., & Loveday, J. 1990, MNRAS, 242, 43P
Matarrese, S., Verde, L., & Heavens, A. F. 1997, MNRAS, 290, 651
Mo, H. J., Jing, Y. P., & White, S. D. M. 1997, MNRAS, 284, 189
Mo, H. J., & White, S. D. M. 1996, MNRAS, 282, 347
Nariai, H. 1969, Prog. Theor. Phys., 42, 544
Peebles, P. J. E. 1980, The Large-Scale Structure of the Universe (Princeton: Princeton Univ. Press)
———. 1993, Principles of Physical Cosmology (Princeton: Princeton Univ. Press)
———. 1999a, ApJ, 510, 523
———. 1999b, ApJ, 510, 531
———. 2000, ASP Conf. Ser. 200, Clustering at High Redshift, ed. A. Mazure, O. Le Fevre, & V. Ke Brun (San Francisco: ASP), 377
Press, W. H., & Schechter, P. 1974, ApJ, 187, 425
Robinson, J., Gawiser, E., & Silk, J. 1998, ApJL, submitted (preprint astro-ph/9805181)
Santiago, D. I., Kalligas, D., & Wagoner, R. V. 1997, Phys. Rev. D, 56, 7627
Scoccimarro, R. 2000, ApJ, 542, 1
Scoccimarro, R., Colombi, S., Fry, J. N., Frieman, J., Hivon, E., & Melott, A. 1998, ApJ, 496, 586
Scoccimarro, R., Couchman, H. M. P., & Frieman, J. 1999, ApJ, 517, 531
Scoccimarro, R., & Frieman, J. 1996, ApJS, 105, 37
Scoccimarro, R., Sheth, R., Hui, L., & Jain, B. 2000, ApJ, 546, 20
Sheth, R. K., & Lemson, G. 1999, MNRAS, 304, 767
Szapudi, I., Colombi, S., Bernardeau, F. 1999, MNRAS, 310, 428
Szapudi, I., Dalton, G. B., Efstathiou, G., & Szalay, A. S. 1995, ApJ, 444, 520
Wald, R. M. 1984, General Relativity (Chicago: Univ. Chicago Press)
Weinberg, S. 1972, Gravitation and Cosmology (New York: Wiley)
White, M. 1999, MNRAS, 310, 511
White, S. D. M., Efstathiou, G., & Frenk, C. S. 1993, MNRAS, 262, 1023
Will, C. M. 1993, Theory and Experiment in Gravitational Physics (2d Ed.; Cambridge: Cambridge Univ. Press)
Willick, J. A. 2000, ApJ, 530, 80